EURASIAN JOURNAL OF MATHEMATICAL AND COMPUTER APPLICATIONS
ISSN 2306–6172
Volume 13, Issue 4 (2025) 141 – 158

EFFECT OF CONVECTION ON IMPURITY TRANSPORT THROUGH POROUS MEDIUM IN HORIZONTAL DIRECTION

Khabin M.R. [1], **Belyaeva A.V.**, **Maryshev B.S.**

Abstract The paper compares the results of numerical modeling with experimental data obtained as a result of a series of experiments to study. The pumping of a finite volume of solution through an elongated rectangular domain of a porous medium is modeled. The MIM approach is used to describe the transport of the impurity. The sorption process is described by a nonlinear MIM model with saturation. Density heterogeneity due to concentration differences is taken into account in the Darcy-Boussinesq approximation. Clogging of the medium due to the deposition of dissolved matter on the pore wall leading to a decrease in porosity, which in turn leads to a decrease in permeability. The dependence of permeability on porosity is given by the Kozeny-Carman equation. The model parameters were found for which the modeling results are in good agreement with the experimental data. The influence of model parameters on breakthrough curves was analyzed. The fields of concentration distribution and current function at different time moments has been received, they demonstrate the occurrence and development of concentration convection in the system.

Keywords: solute convection, numerical modeling, clogging, immobilization.

AMS Mathematics Subject Classification: Classification codes 76S05, 76M20, 76R10.

DOI: 10.32523/2306-6172-2025-13-4-141-158

1 Introduction

In the course of production and industrial activities, people have to face difficulties in the exploitation of natural geological systems. Geological systems are represented by various rocks and soils which can be described as porous media. During the filtering process of any mixture through such media the particles of the solid matrix and impurities distributed into the media can interact with pore wall. Such interaction significantly complicates the description of fluid transport through porous media. The transport of solutes into porous media is typically characterized by the immobilization of impurities through deposition onto the solid matrix of the medium. The immobilisation may be caused by various reasons. It can be mechanical blockage of pore [1], chemical reaction [2], physical sorption [3, 4] etc. But most common example of immobilisation is the electrical interaction of impurity with the pore wall caused by van der Waals forces.

The popular continuous media approach to model the transport through porous media with immobilization is mobile/immobile medium (MIM) [5]. The main idea of MIM approach is the separating an impurity into two phases: mobile (free) and immobile (adsorbed on pore walls). The mobile impurity can move with the fluid flow or by diffusive mechanism. The immobile impurity interact with pore wall and this impurity cannot move. In this case, the transport of the impurity is provided by the immobile phase. It is described using the standard advection diffusion model [6] for a mobile impurity with an additional term that models the

[1]Corresponding Author.

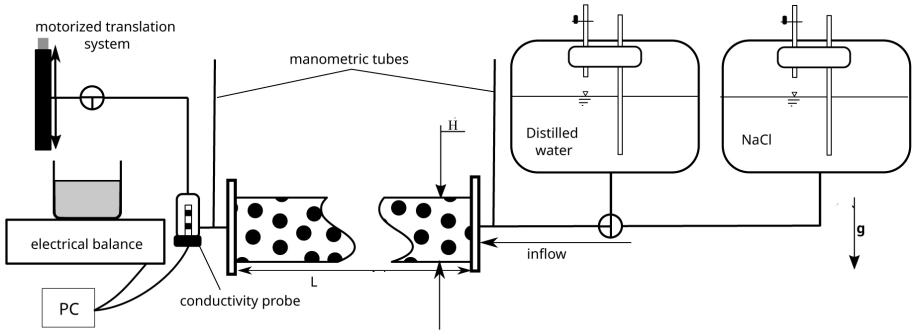

Figure 1: Schematic diagram of the laboratory column apparatus.

influx of the impurity into the immobile phase. The exchange of impurity between phases is usually described by additional kinetic equation. The mathematical form of such equation depends on the nature of the interaction of impurity with solid matrix of porous media.

The most popular model with description of such interaction as the physical sorption caused by van der Waals forces is known as standard or linear MIM model [7]. This model based on linear dependence between the influx of impurity and admixture volumic concentrations in both phases. It means that the influx of impurity to immobile phase linearly increases with mobile concentration increasing and linearly decreases with immobile concentration increasing. This model contains two empiric parameters: adsorption and desorption rates. The linear model is well verified by experimental data [8, 9] for small impurity concentrations. In the case of significant concentrations the adsorption process should be limited because the capacity of immobile phase is finite. This feature is taken into account in nonlinear model with limited immobile concentration [10] when the concentration of adsorbed impurity cannon exceed some value. Such limit concentration becomes the additional empiric parameter of transport model.

The estimation of transport model parameters is very important problem which should be solved for application of such transport model to real industrial problems and the prediction of such geological phenomena. Usually the data for parameter estimation are obtained from the experiments of mixture portion transport through porous column [12, 13, 14]. Such data are breakthrough curves (BTC), it is the dependence of impurity concentration on time in some section of the column, most often at outlet. The longitudinal scale of the column usually much greater then transverse because of the filtration flow is assumed as one dimensional. Such assumption allows measuring only the full concentration into cross section of column and compare the obtained BTC with the solution of one dimensional problem within MIM approach (see [11]). However, it is known that the convection in porous media is recognized in the presence of any (even extremely small) horizontal heterogeneity of density [15, 16]. The convective motion made the flow two or three dimensional everywhere. The intensity of convection is proportional to impurity concentration into the mixture. In the case of small concentrations it is believed that taking into account convection is not necessary [12, 13].

The present study is devoted to analysis of convection properties and it impact to transport process in porous media for significant impurity concentration. The interest of authors is application the MIM approach to transport problems for wide range of concentrations also with parameter estimation (see [11]). Here we solve numerically the two dimensional problem within the nonlinear MIM approach for modeling the standard transport experiment.

2 Experiment

The experiments were made with a horizontally oriented acrylic cylinder of 500 mm length L and 16 mm internal diameter d. Quartz sand with fraction size of 0.8-1.2 mm was used as a porous medium. The column was packed under a wet condition as uniformly as possible. Porous brass plates at a both ends of the column kept the sand out. Aqueous solutions of NaCl at different initial mass concentration were used as contaminant. The inflow apparatus consisted of two chambers with a constant head of distilled and salt water. These chambers were connected to the inlet of the column by a three-way valve, which enabled manual switching between the distilled and salt water circuit. The brine was injected in the column while maintaining a constant mass flow rate. The duration of step brine injection depends on the initial flow rate and corresponds to the introduction of about 10% of the column pore volume. The mass of outflowing fluid was measured with electronic precision balance. The concentration of NaCl in outflowing fluid was measured by on-line electric conductivity cell. A diagram of the column apparatus is given in Fig. 1. To realize the control of constant filtration flow rate , the column outlet was connected to a motorized translation system that allows changing the pressure level at the outlet. The translation system software allows remote control of vertical coordinate, maximum speed and acceleration of outlet valve travel.

3 Problem statement. Seepage with constant flow rate

Let us describe the transport of mixture through porous column. The problem is solved in a two-dimensional formulation. A portion of the mixture with a volume about 10% of the pore space volume is pumped through a rectangular domain of the porous medium in the gravity field. The aspect ratio of the domain $H/L = 0.1$. Horizontal filtration rate remains constant. Horizontal boundaries of the area are impermeable for the carrier liquid and impurity. At the inlet of column (left side) the condition of given impurity flux is posed, at the outlet (right side) the free flow condition is used. The sketch of the problem is presented in fig.2.

The problem is solved within framework of the MIM (mobile/immobile media) approach [5]. The main idea of this approach is separating the impurity into mobile and immobile components. The mobile component can move with the carrier fluid, while the immobile component interacts (settle) on the pore walls. This approach implies the existence of a kinetic equation describing the impurity transition between the components, i.e. sorption process. Concentration variation in an elementary volume of porous medium is determined by the law of mass conservation. The detailed derivation of the all governing equations can be found [17]. Mathematically, it can be written as

$$\frac{\partial(\phi C + Q)}{\partial t} = -\operatorname{div} \mathbf{J},$$

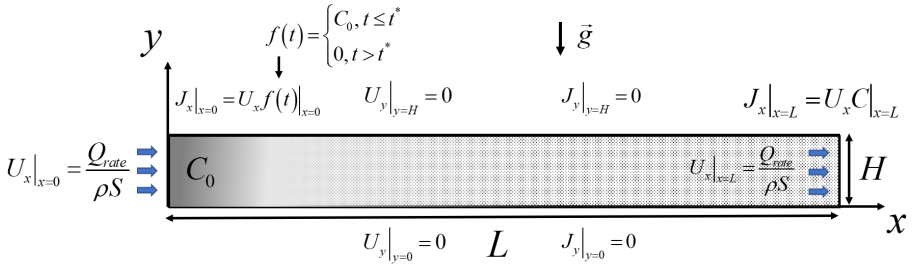

Figure 2: Sketch of the problem.

where C - volumic concentration of mobile component, Q - volumic concentration of immobile component, ϕ - current porosity of porous medium, $\mathbf{J}$ - the flux of impurity. The flux contains two parts diffusive and advective:

$$\mathbf{J} = -\phi D \nabla C + \phi \mathbf{W}\, C = -\phi D \nabla C + \mathbf{U}\, C, \tag{1}$$

where $\mathbf{W}$ is pore velocity and $\mathbf{U} = \phi \mathbf{W} = (U_x, U_y)$ is filtration velocity vector, D is effective diffusivity.

In the present work, the nonlinear kinetic equation [10] is used due to significant concentration C_0 of impurity in transported portion. This equation takes into account the fact that there is some limiting value of impurity concentration into the immobile component. Mathematically it can be presented as

$$\frac{\partial Q}{\partial t} = \alpha((Q_0 - Q)C - K_d Q), \tag{2}$$

where α is the mass transport coefficient, K_d is the solute distribution coefficient, Q_0 is the limit concentration of the immobile phase. Filtration flow through a porous column is described by the Darcy law [18], in form of

$$\mathbf{U} = -\frac{\kappa(\phi)}{\eta}(\nabla P' + \rho \mathbf{g}), \tag{3}$$

where κ is the permeability of the porous medium, η is the dynamic viscosity of fluid, ρ is the fluid density, P' is the pressure, $\mathbf{g} = -g\,\mathbf{k}$ is the gravity acceleration vector ($\mathbf{k}$ is the unit vector of y-axis). The impurity accumulation into immobile phase reduces the actual pore volume. Using the standard definition of immobile impurity concentration (Q) like the ratio ($Q = V_i/V$) between the volume occupied the immobile impurity (V_i) and the full volume of media (V), one can write the dependence of porosity (ϕ) on Q in form of

$$\phi = \phi_0 - Q, \tag{4}$$

where ϕ_0 is the porosity of clean media without any impurity. The reduction of pore volume and decreasing of porosity leads to increasing of hydraulic resistance of medium. This process is called the clogging of porous media and can be described by the dependence of media permeability on porosity. Here the most popular expression in form of Kozeny-Karman equation [19] is used

$$\kappa(\phi) = \gamma \frac{\phi^3}{(1-\phi)^2}, \tag{5}$$

with γ is the Kozeny-Carman constant. The Kozeny-Carman constant is empirical parameter which can be measured for a clean medium.

For the description of convective flow the heterogeneity of fluid density due to variation of impurity concentration in mobile phase should be taken into account. The experiments [20] shown that the significant values of concentration in sense of porous media clogging are not so big. It is allow us to the Bousinesq approximation [18] of the density dependence on the concentration of impurity in linear form:

$$\rho(C) = \rho_0(1 + \beta_C C), \tag{6}$$

where ρ_0 is the density of carrier liquid, β_C is the coefficient of concentration expansion. It is assumed that the fluid is incompressible

$$\operatorname{div} \mathbf{U} = 0 \tag{7}$$

The equations (3) and (6) can be combined

$$\mathbf{U} = -\frac{\kappa(\phi)}{\eta}(\nabla P' - \rho_0 g \beta_C C \mathbf{k}), \quad P = P' - \rho_0 g y \tag{8}$$

with P is the deviation of pressure from the hydrostatic one. Thus, we have the following system of equations:

$$\begin{gathered}\frac{\partial(\phi C+Q)}{\partial t}=-\mathrm{div}(-\phi D\nabla C+\mathbf{U}C),\quad \frac{\partial Q}{\partial t}=\alpha((Q_0-Q)C-K_dQ),\\ \mathrm{div}\mathbf{U}=0,\quad \mathbf{U}=-\frac{\kappa(\phi)}{\eta}(\nabla P-\rho_0 g\beta_C C\mathbf{k}),\quad \kappa(\phi)=\gamma\frac{\phi^3}{(1-\phi)^2},\quad \phi=\phi_0-Q,\end{gathered}\tag{9}$$

with boundary conditions

$$\begin{gathered}J_x\mid_{x=0}=U_x\mid_{x=0}f(t),\quad f(t)=\begin{cases}C_0, & t\le t^*\\ 0, & t>t^*\end{cases}\\ J_x|_{x=L}=U_xc|_{x=L},\quad U_x|_{x=0,L}=Q_{rate}/\rho_0 S,\quad U_y|_{y=0,H}=0,\quad J_y|_{y=0,H}=0.\end{gathered}\tag{10}$$

where J_x is horizontal component of impurity flux, $f(t)$ is step function of time, Q_{rate} is constant filtration rate which is controlled in experiment, S is the area of column cross section. The boundary conditions correspond to standard conditions which is applied in experiment (see Section 2). At inlet ($x=0$) the impurity flux is given by step function of time. This condition is modelled the pumping of mixture portion. The outlet condition ($x=L$) the free flow condition is applied. The horizontal boundaries is assumed impermeable for carrier liquid and impurity.

It is convenient to rewrite the equations (9) with the boundary conditions (10) in dimensionless form using the next scales for measuring distance, time, velocity, permeability, pressure, saturated concentration immobile phase and concentration as L, L^2/D, $\phi_0 D/L$, γ, $Q_{rate}\eta L/\rho S\gamma$, Q_0, C_0

$$\begin{gathered}\frac{\partial c}{\partial t}+\frac{\zeta}{C_0}\frac{\partial q}{\partial t}-\zeta\frac{\partial(qc)}{\partial t}=(1-\zeta q)\Delta c-\zeta(\nabla q\nabla c)-\mathbf{u}\nabla c,\quad \frac{\partial q}{\partial t}=a(1-q)c-bq,\\ \mathrm{div}\mathbf{u}=0,\quad \mathbf{u}=-\kappa(\phi)(\mathrm{Pe}\nabla p+\mathrm{Rp}\,c\mathbf{k}),\quad \kappa(\phi)=\frac{\phi^3}{(1-\phi)^2},\quad \phi=\phi_0(1-\zeta q),\end{gathered}\tag{11}$$

where c, q and p are dimensionless values of mobile and immobile impurity concentrations and pressure. The $\mathbf{u}=(u_x,u_y)$ is vector of dimensionless filtration velocity. Equations (11) contains five dimensionless parameters: the diffusive analogue of Peclet number $\mathrm{Pe}=(Q_{rate}L)/(\rho_0 S\phi_0 D)$, the Rayleigh-Darcy number $\mathrm{Rp}=(\gamma\rho_0 g\beta_C C_0 L)/(\phi_0\eta D)$, the clogging parameter $\zeta=Q_0/\phi_0$, the adsorption $a=\alpha C_0 L^2/D$ and desorption $b=\alpha K_d L^2/D$ rates.

Let us introduce the current function in terms $u_x=\partial\psi/\partial y$, $u_y=-\partial\psi/\partial x$. In the approach of a weak clogging ($\zeta\ll 1$) the equations (11) can be rewritten in the terms of current function as

$$\begin{gathered}\frac{\partial c}{\partial t}+\frac{\zeta}{C_0}\frac{\partial q}{\partial t}=\frac{\partial^2 c}{\partial x^2}+\frac{\partial^2 c}{\partial y^2}-\frac{\partial\psi}{\partial y}\frac{\partial c}{\partial x}+\frac{\partial\psi}{\partial x}\frac{\partial c}{\partial y},\quad \frac{\partial q}{\partial t}=a(1-q)c-bq,\\ \frac{\partial^2\psi}{\partial x^2}+\frac{\partial^2\psi}{\partial y^2}-\frac{1}{\kappa(\phi)}\frac{\partial\kappa}{\partial\phi}\left(\frac{\partial\phi}{\partial x}\frac{\partial\psi}{\partial x}+\frac{\partial\phi}{\partial y}\frac{\partial\psi}{\partial y}\right)=\kappa(\phi)\mathrm{Rp}\frac{\partial c}{\partial x},\quad \kappa(\phi)=\frac{\phi^3}{(1-\phi)^2},\quad \phi=\phi_0(1-\zeta q).\end{gathered}\tag{12}$$

The weak clogging approach (see [21]) can be applied if the clogging parameter is small $q\zeta\lesssim 0.1$ where q is characteristic value of dimensionless immobile concentration. In this case we can exclude all terms with ζ except two terms. First (I) is $\zeta/C_0\sim 1$ they usually have the same order, second (II) in the Kozeny-Carman expression because the small variations of porosity leads to significant variations of permeability (the minimal possible ratio is about 10, see [21]) .

Let us rewrite the boundary conditions (10) in terms of the current function:

$$
\begin{aligned}
&J_x|_{x=0} = \left.\frac{\partial\psi}{\partial y}\right|_{x=0} f(t), \quad f(t) = \begin{cases} 1 & \text{if } t \le t^* \\ 0 & \text{if } t > t^* \end{cases}, \\
&J_x|_{x=1} = \left.\frac{\partial\psi}{\partial y}c\right|_{x=1}, \quad \left.\frac{\partial\psi}{\partial y}\right|_{x=0,1} = \mathrm{Pe}, \quad \left.\frac{\partial\psi}{\partial x}\right|_{y=0,h} = 0, \quad J_y|_{y=0,h} = 0,
\end{aligned}
\tag{13}
$$

initial conditions are set by absence of impurity inside the region and constant filtration rate

$$
c(x, y, t = 0) = 0, \quad q(x, y, t = 0) = 0, \quad \psi(x, y, t = 0) = \psi_0(y) = \mathrm{Pe}\, y, \tag{14}
$$

the last expression for stream function correspond to solution of one dimensional problem of fluid filtration without any impurity The equations (12) with boundary conditions (13) and initial conditions (14) is solved numerically. The details of numerical method is presented into appendix. The next section is devoted to discussion about obtained solutions, to comparison with experimental data and analysis of parameter variation to observed convective motion.

4 Results and discussion

In present section we present the results of numerical solution of problem (12)–(14). First of all we verify our model by the comparison with experimental data.

4.1 Comparison with experiment

The BTC plotted in dimension form for better and convenient comparison the results of numerical calculation with experimental data. The experimental data contain only BTC at outlet of porous column which obtained for porous column in form of cylindrical pipe. The calculation is provided for two dimensional rectangular domain because of that the numerical and experimental are not the same. For recalculation of two dimensional data to integral BTC concentration at the outlet of the porous column is defined as follows

$$
\begin{aligned}
V_{imp}(t) &= \int_0^L\int_0^H [\phi(x, y, t)C_0 c(x, y, t) + Q_0 q(x, y, t)]dxdy, \\
C_{\mathrm{out}}(t) &= \frac{\rho_{imp}}{\phi U S}\,\frac{V_{imp}(t+\Delta t) - V_{imp}(t)}{\Delta t},
\end{aligned}
\tag{15}
$$

where V_{imp} is volume into the column occupied by impurity, $U = \mathrm{Pe}\phi_0 D/L$ is filtration rate, $\phi(x, y, t)$ is the current porosity, $\Delta t = \tau L^2/D$ is the dimension time interval, τ is the time grid step of used numerical method (see Appendix), ρ_{imp} is density of impurity.

Different types of concentrations can be found in the literature: volumetric (C_{vol}), mass (C_{mass}) or expressed in mass per unit volume ($C_{m/V}$). These concentrations are related to each other $C_{m/V} = \rho_{sol}C_{mass} = \rho_{imp}C_{vol}$, where ρ_{sol} is the solution density. The concentrations C, Q and C_0 are volumetric because the governing equations (9) is derived for such type of concentrations. The volumetric concentrations C and Q are calculated and converted to a outlet concentration in grams per liter (C_{out}) for comparison with experimental data (see Eq. (15)). Also the value mass concentration C_{in} at inlet (from experimental data) is converted to volumetric C_0 when the parameters of model is estimated (see Tab. 3).

The selection of transport parameters values is based on parameter identification method which is presented in [11]. This method contain the solution of one dimensional problem any convection. Instead of that the experimental data about the dependence of pressure drop between column ends on time during the transportation process is used for parameters estimation. The method allow us to estimate four parameters: diffusivity (D), mass transport coefficient (α), solute distribution coefficient(K_d) and limit concentration of immobile phase (Q_0).

The used porous material is quartz sand with porosity $\phi_0 \approx 0.48$ and permeability of clean media $\kappa(\phi_0) \approx 3.1 \cdot 10^{-10}\mathrm{m}^2$ which give as the Kozeny-Carman constant value $\gamma \approx 0.79 \cdot 10^{-9}\mathrm{m}^2$. The porous column is a cylindrical tube with length $L = 0.5$ m and cross section area $S \approx 2\,\mathrm{cm}^2$. The carrier liquid is water with dynamic viscosity $\eta \approx 10^{-3}\,\mathrm{Pa}\,s$ and density $\rho_0 = 10^3\,\mathrm{kg/m}^3$. The impurity is sodium chloride (NaCl) with density $\rho_{imp} = 2.16 \cdot 10^3\,\mathrm{kg/m}^3$ and the density of $NaCl$ solute in water (up to near 15% of mass concentration) can be presented by linear approximation [20] with coefficient of concentration expansion $\beta_C = 1.55$ (see Eq. (6)).

The two realisations of experiment with close values of flow rate (dimensionless Peclet diffusion number) and different initial concentrations of impurity (C_0) are described. The difference in concentration leads to the same significant difference in Raleigh-Darcy number. The last parameter is define the intensity of convective motion. It means that two described cases corresponds to (I) moderate and (II) high intensities of convective motion. The parameters for both realizations are presented in Tab. 3.

The comparison of numerical calculation results with BTC's obtained by experiment is presented in Fig. 4.

It is seen from Fig. 4 that form of curves (blue and black) are close. Some discrepancy between curves can be explained by difference between model problem (12)-(14) and experimental setup. The form of BTC corresponds to the standard form within MIM model the peak of concentration provides by mobile phase transportation and very slow decline (tail of BTC) is provided by slow transport of impurity that initially transits to immobile phase. The convective motion can be illustrated by fields of concentration and stream function much better than by BTC. The evolution of concentration field during the transport process for the same with realisation (II) parameter values (see Tab. 3) is shown in Figs. 5 and 6.

Figs. 5 and 6 demonstrated that transport regime for mobile concentration very close to one dimensional solution, weak of isolines can be observed only at back front of concentration impulse (see the field at t=480 seconds). The isolines of immobile concentration is more inclined because its moving is slower and realized only by the impurity transition to mobile phase. The convective motion is most clearly visible in analysis of stream function field (see fig. 7).

In Fig. 7 shown the evolution of two dimensional vortex. This vortex is being formed at initial stage of transportation process and growth in time. At the final stage the convective cell with inverse vortex (near inlet) can be observed.

The next subsection is devoted to analysis the impact of transport parameter variation to observed convective motion and the effect of last motion effect to transportation process.

4.2 Analysis of parameter variation

In this section presented and discussed the results of numerical calculation for different values of transport parameters. Some values chosen close to experimental (see Tab. 3) another far from its for better demonstration of possible effects. All effects shown by two ways first is the appropriate BTC and second the variation the stream function field as visual identifier of convective motion.

The breakthrough curves for various values of adsorption and desorption rates are presented in fig. 8

It is seen from Fig. 8 (a) that increasing in adsorption rate (a) value leads to decreasing of primary peak (or first peak) of BTC. The first peak is observed due to advective transport of mobile impurity which has not transit into immobile phase. The higher values of adsorption rate intensify the transition of impurity to immobile phase and amount of mobile impurity reduced. However, this effect is accompanied by a growth of secondary peak. Such peak and

Figure 3: The transport parameters for two experimental realisations (Section *Measured* contain the parameters which are measured directly, next section *Estimated* contain the values of estimated by method [11] parameters and the last section *Dimensionless* contain the appropriate values of dimensionless parameters which are used for numerical calculations).

Parameter name	Realisation (I)	Realisation (II)
Measured		
Q_{rate}, g/s	0.051	0.054
t^*, s	94	89
C_{in}, % of mass	5	10
Estimated		
$D \cdot 10^7$, m^2/s	4.24	4.31
$\alpha \cdot 10^3$, 1/s	5.81	6.12
K_d	0.32	0.36
Q_0	0.16	0.17
Dimensionless		
Pe	627	653
Rp	723	1450
a	83	174
b	1096	1233
ζ	0.34	0.36

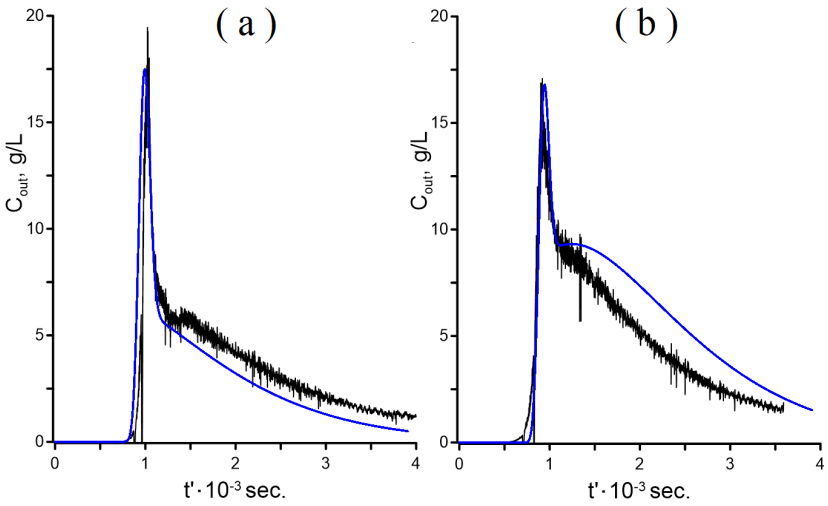

Figure 4: Breakthrough curves at the outlet of the column for mass concentration. The concentration is calculated by expressions (15), the time is presented in dimensional form as $t' = tL^2/D$. Plot (a) realisation (I) and (b) realisation (II), the blue curve is result of numerical calculation with dimensionless parameters and black curve is experimental data.

moreover the presence of "heavy tail" (very slow decline of concentration in time) at BTC is caused by removal of immobile impurity from porous column. The last removal is very slow because the impurity multiple transits between two phases and it moves only in mobile one. The increasing in desorption rate value (b) demonstrates the inverse effect: the primary peak growth and decline of concentration at the "tail" of BTC speeds up (see Fig. 8 (b)).

Figs. 9 and 10 demonstrate the effect of sorption rates variation to structure of convective motion. It is seen (Fig. 9) that the enlargement of adsorption rate leads to slow down of convective motion and simplification of field structure. This effect can be explained by the

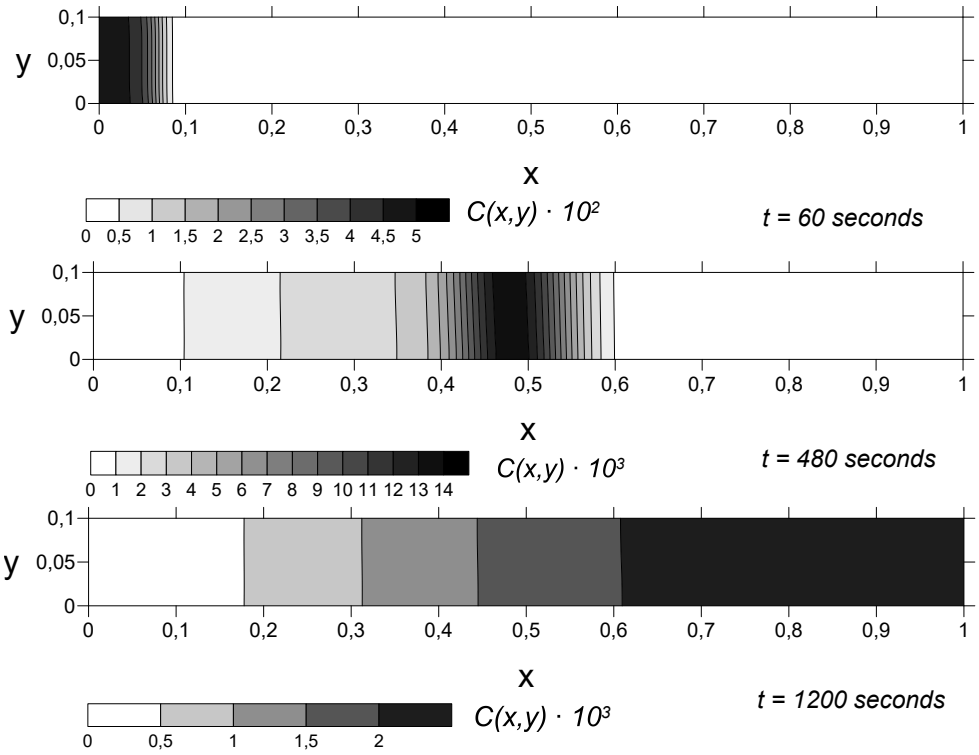

Figure 5: The calculated field of mobile concentration for parameter values of realisation (II) (see Tab. 3)

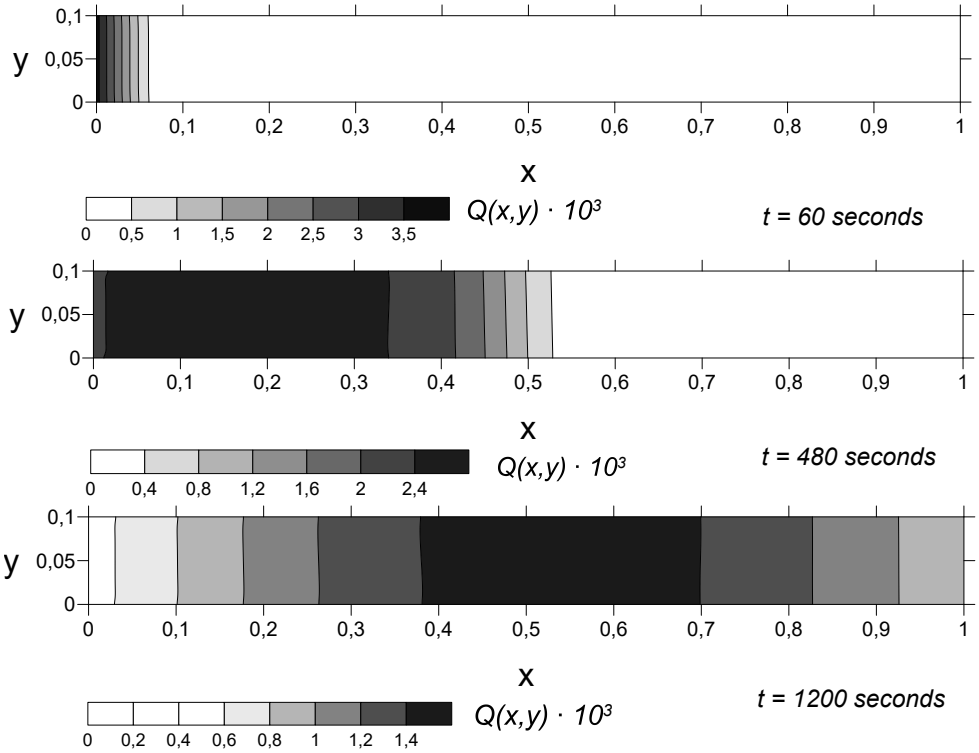

Figure 6: The field of immobile concentration for parameter values of realisation (II) (see Tab. 3).

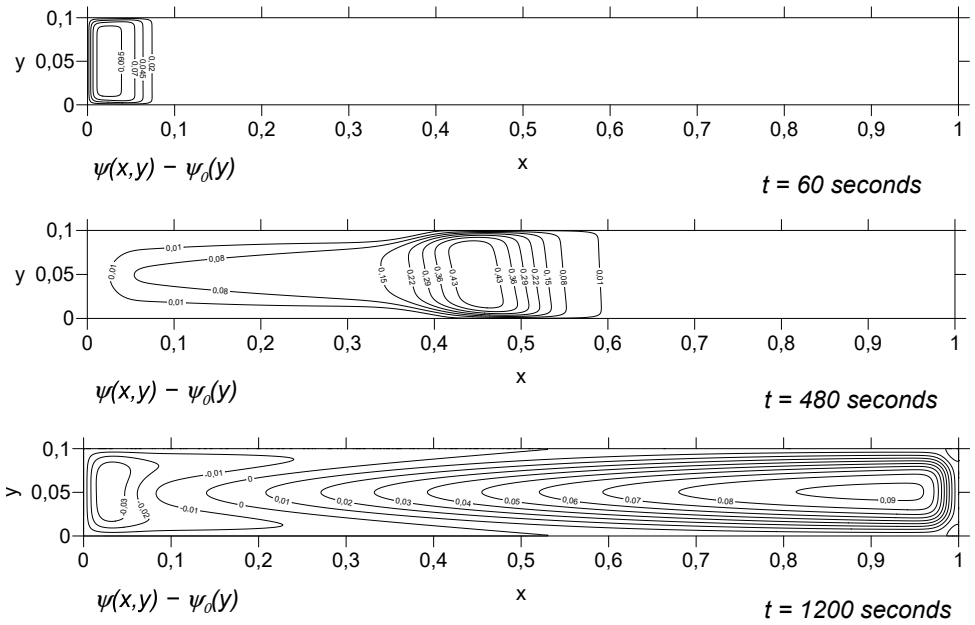

Figure 7: The field of current function perturbation $(\psi - \psi_0)$, where $\psi_0 = \mathrm{Pe}\, y$ for parameter values of realisation (II) (see Tab. 3).

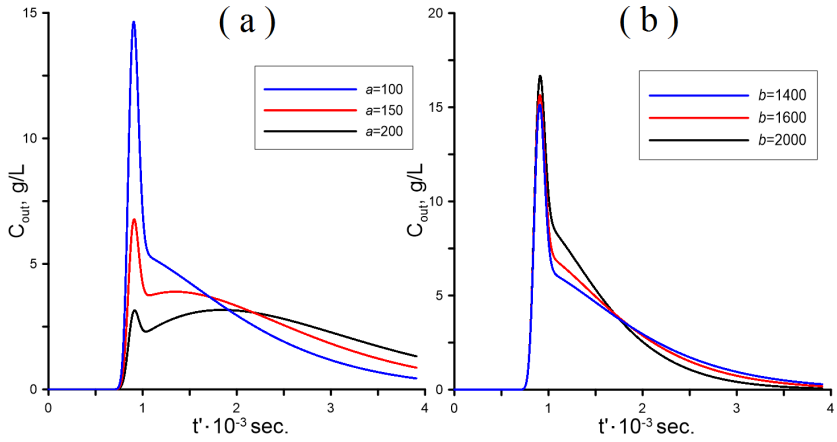

Figure 8: Dependence of the concentration at outlet on time (BTC) for various values of sorption parameters, the time is presented in dimensional form as $t' = tL^2/D$, where $D = 4.2 \cdot 10^{-7}\mathrm{m}^2/\mathrm{s}$ and $L = 0.5\, m$. The curves on panel (a) is calculated for desorption rate $b = 1200$ and for different values of adsorption rate a (indicated in legend), the plots (b) is calculated for adsorption rate $a = 100$ and various values of desorption rate b (indicated in legend). Another parameter values are $C_0 = 5\%$ of mass, $\mathrm{Pe} = 700$, $\mathrm{Rp} = 6000$, $\phi_0 = 0.48$, $\zeta = 0.3$, $t^* = 86$ s.

depletion of mobile phase. The density heterogeneity of filtering mixture is the main reason of convection, but when some part of impurity transits to immobile phase then the impurity concentration in filtering mixture decreases and density becomes more homogeneous. The increasing into the values of desorption rate (b) leads to inverse effects (see Fig. 10).

The BTC variation with changing of Peclet and Rayleigh-Darcy values is shown in Fig. 11

It is demonstrated in Fig. 11 that decreasing of Peclet number leads to reduce the primary peak and enlarge the time of its observation, the secondary peak also growth. Additionally for smaller Peclet number value the appropriate injection time becomes greater (see Fig. 11 (a). The enlargement of injection and peak observation times are caused by the slow down of

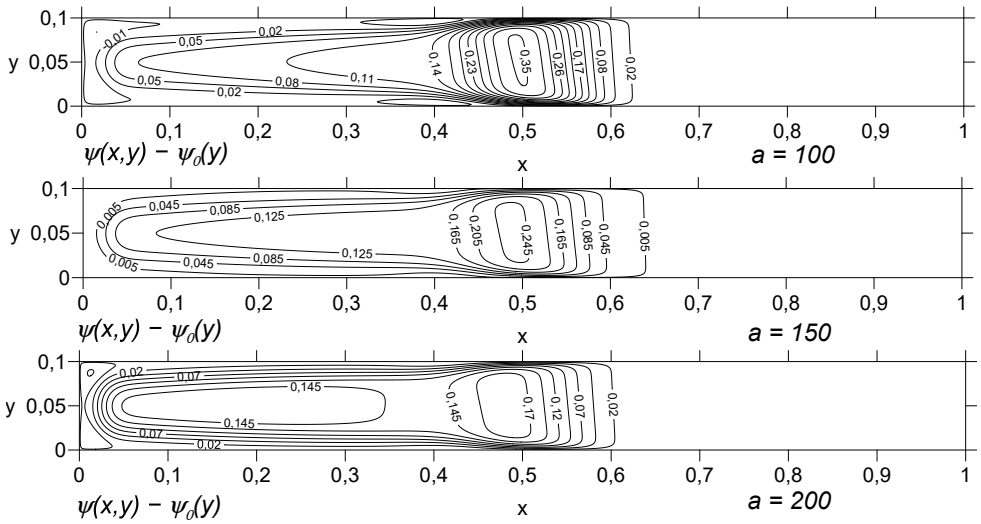

Figure 9: The fields of current function perturbation $(\psi - \psi_0)$, where $\psi_0 = \mathrm{Pe}\, y$. The calculation is performed for different values of adsorption rate (a), another parameter values are: $\mathrm{Pe} = 700$, $\mathrm{Rp} = 6000$, $b = 1200$, $\phi_0 = 0.48$, $\zeta = 0.3$, $t^* = 86$ s at the dimensional time moment $t' = 480$ s.

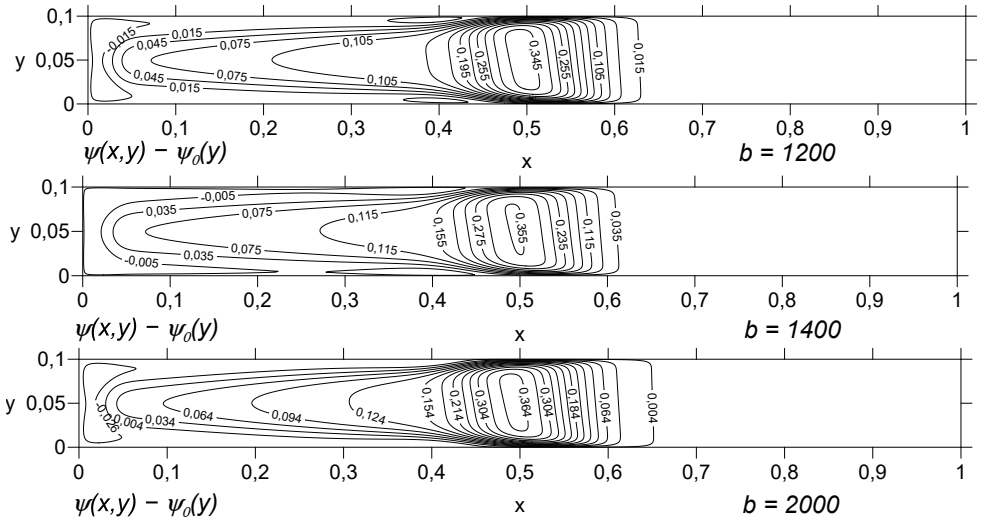

Figure 10: The fields of current function perturbation $(\psi - \psi_0)$, where $\psi_0 = \mathrm{Pe}\, y$. The calculation is performed for different values of desorption rate (b), another parameter values are: $\mathrm{Pe} = 700$, $\mathrm{Rp} = 6000$, $a = 100$, $\phi_0 = 0.48$, $\zeta = 0.3$, $t^* = 86$ s at the dimensional time moment $t' = 480$ s.

filtration process. The Peclet number is dimensionless filtration flow rate and its decreasing leads to growth of all filtration times. The greater time of transport process gives more time for immobilization process. One can observe the enlargement in immobile concentration and secondary BTC peak as consequence. The increasing in Rayleigh-Darcy value (see Fig. 11 panel B) reduces only the maximal concentration in primary peak at BTC due to intensification of convection and small slow down the filtration troughflow at constant flow rate (Peclet number). Such a small effect of Rp variation can be explained by the form of porous column, the longitudinal size is much greater than vertical ($l = H/L \ll 1$). The third equation in (11) show that filtration velocity u consist of two terms: first is advective term which is proportional to Peclet number and caused by horizontal pressure drop. This term provides

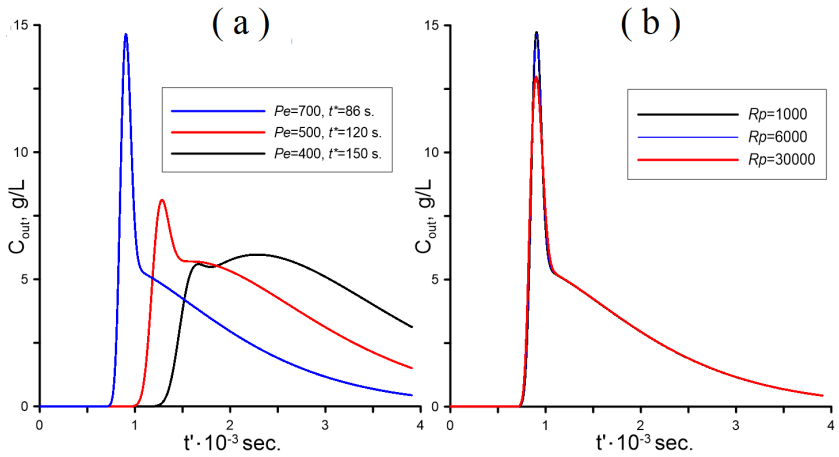

Figure 11: Dependence of the concentration at outlet on time (BTC) for various values of Peclet and Rayleigh-Darcy numbers, the time is presented in dimensional form as $t' = tL^2/D$, where $D = 4.2 \cdot 10^{-7}$ m^2/s and $L = 0.5$ m. The curves on panel (a) is calculated for Rayleigh-Darcy number Rp = 6000, for different values of Peclet number Pe and times of injection $t*$ (indicated in legend), the plots (b) is calculated for Peclet number Pe = 700, $t^* = 86$ s and various values of Rayleigh-Darcy number Rp (indicated in legend). Another parameter values are: $C_0 = 5\%$ of mass, $a = 100$, $b = 1200$, $\phi_0 = 0.48$, $\zeta = 0.3$.

mainly the horizontal component of filtration velocity. The second term is convection part. It is vertical component of velocity which is proportional to Rayleigh-Darcy number and density field heterogeneity due to mobile concentration. The ratio between horizontal and vertical components of velocity is proportional to the aspect ratio of column $l = 0.1$. It means that the convective motion intensity is in ten times weaker than advective motion at the same values of Pe and Rp. The most visible effect of Rp variation can be demonstrated by the field of current function (see Fig. 13).

Figs. 12 and 13 present the current function dependence on variation of Pe and Rp respectively. It is seen that increasing in Peclet number value leads to spreading of vortex into column due to spreading the front of impurity impulse (see Fig. 12). Into the right part of column there is no impurity and also no heterogeneity of density field. As result the convective motion in form of vortex does not observed. Fig. 12 also demonstrates that the structure of of flow is not changed greatly with variation of Peclet number but intensity of convection increases with decreasing of Pe.

The complication of the convective flow structure with enlargement in Rayleigh-Darcy number value. Convection intensifies, more small vortexes arise and the isolines incline, but the spreading of convection into the column is not observed due to constant Peclet number.

The dependence of BTC on variation of clean media porosity and clogging parameter is shown in Fig. 14.

The increasing in clogging parameter value means the enlargement of solid matrix adsorption capacity, more impurity can be adsorbed. This fact intensify the adsorption process and the primary peak concentration value at BTC becomes lower (see fig. 14 A). Generally the variation of adsorption rate and clogging parameter lead to similar effects. The decreasing of clean media porosity leads to essential decreasing of permeability, e.g. $\kappa(\phi_0 = 0.48)/\kappa(\phi_0 = 0.44) \approx 1.5$. Due to that fact the hydraulic resistance of media increases and effective flow rate becomes lower. The injection time is growing (for the same volume of injected mixture) and time moment for primary peak position also increases. Generally this effect the same

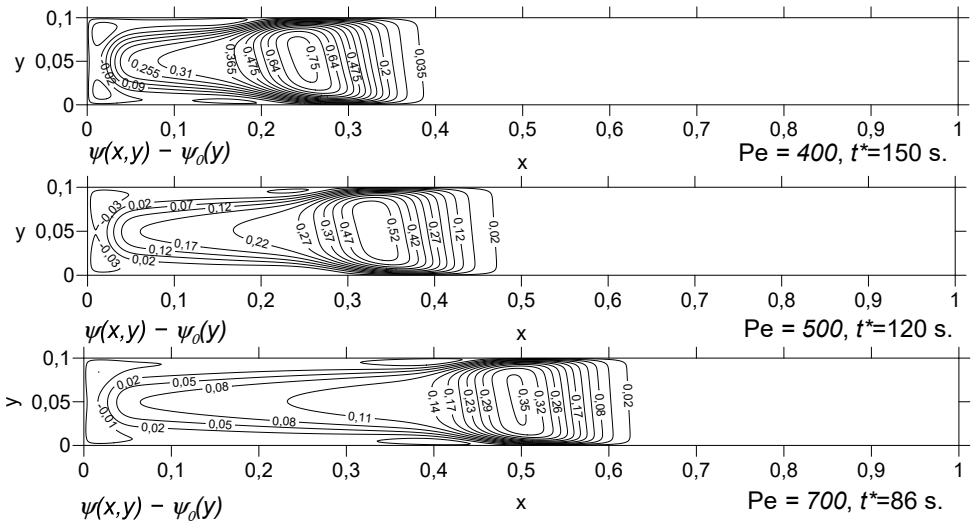

Figure 12: The fields of current function perturbation ($\psi - \psi_0$), where $\psi_0 = Pe\, y$. The calculation is performed for different values of Peclet number (Pe) and injection time ($t*$), another parameter values are: Rp = 6000, $a = 100$ $b = 1200$, $\phi_0 = 0.48$, $\zeta = 0.3$ at the dimensional time moment $t' = 480$ s

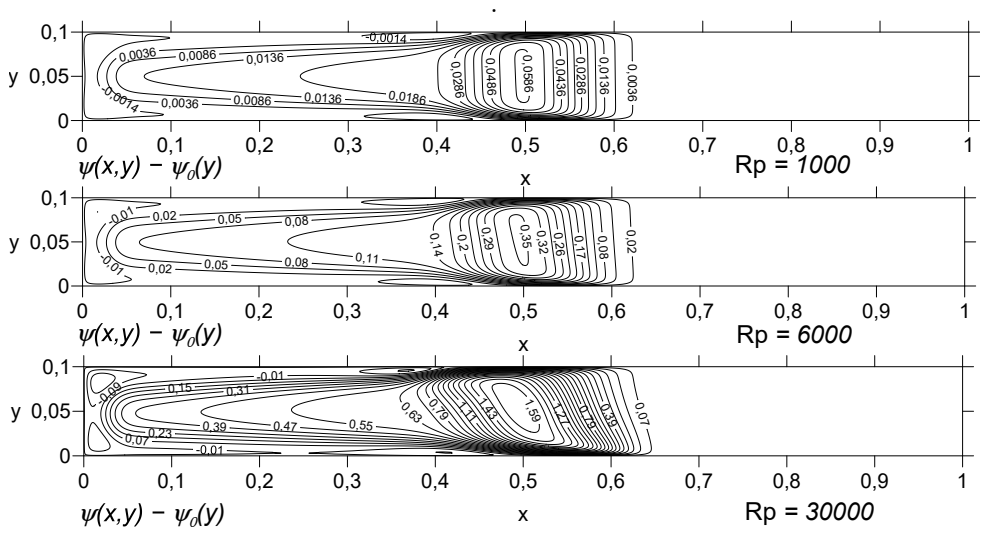

Figure 13: The fields of current function perturbation ($\psi - \psi_0$), where $\psi_0 = \mathrm{Pe}\, y$. The calculation is performed for different values of Rayleigh-Darcy number (Rp), another parameter values are: Pe = 700, $a = 100$ $b = 1200$, $\phi_0 = 0.48$, $\zeta = 0.3$ at the dimensional time moment $t' = 480$ s.

with decreasing the Peclet number. The same effects is demonstrated in Figs.15 and 16 for structure of current function field.

5 Conclusions

The problem of pumping a finite volume of mixture through a rectangular domain of a porous medium is solved. The experimental data for horizontal cylindrical column are compared with the data of the numerical solution. The parameters of the problem that provide the best compliance are estimated. The influence of the parameter variation of the problem on the breakthrough curve and the resulting convective flow is analyzed. It is shown that

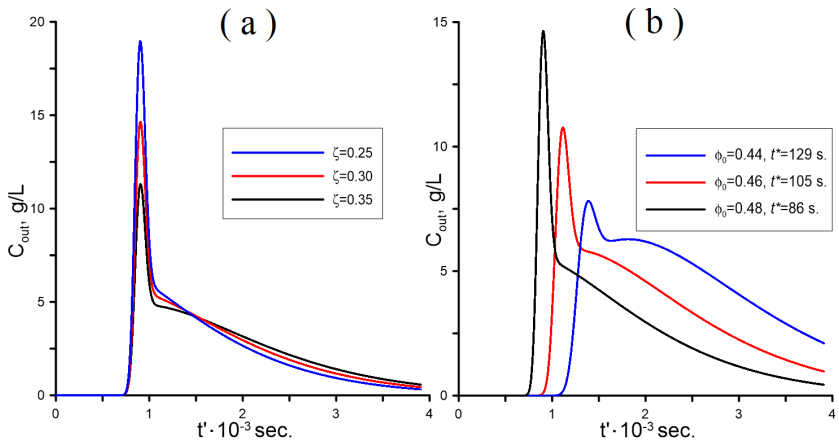

Figure 14: Dependence of the concentration at outlet on time (BTC) for various values of clogging parameters, the time is presented in dimensional form as $t' = tL^2/D$, where $D = 4.2 \cdot 10^{-7}\,\mathrm{m}^2/\mathrm{s}$ and $L = 0.5\,m$. The curves on panel (a) is calculated for clean media porosity $\phi_0 = 0.48$ and $t^* = 86$ s, for different values of clogging parameter ζ (indicated in legend), the plots (b) is calculated for clogging parameter $\zeta = 0.3$ and various values of Rayleigh-Darcy number ϕ_0 and times of injection $t*$ (indicated in legend). Another parameter values are: Pe = 700, Rp = 6000, $C_0 = 5\%$ of mass, $a = 100$, $b = 1200$.

increasing of adsorption rate, clogging parameter and decreasing of desorption rate intensify the adsorption process. It leads to slow down the transport process and convective flow. The primary concentration peak at BTC reduces but the concentration values at BTC "tail" are growing. The increasing of Peclet number and porosity demonstrate the same effect, it is intensification of filtration throughflow. Such intensification speed up the transport process all specific times are decreasing, the convective vortex spreads faster into the column but the intensity of convection is reducing. The variation of Rayleigh-Darcy number has weak effect to BTC. However the enlargement of Rp intensify the convective motion and complicates the flow structure.

Acknowledgement

The work is supported by Russian Science Foundation, project number 20-11-20125.

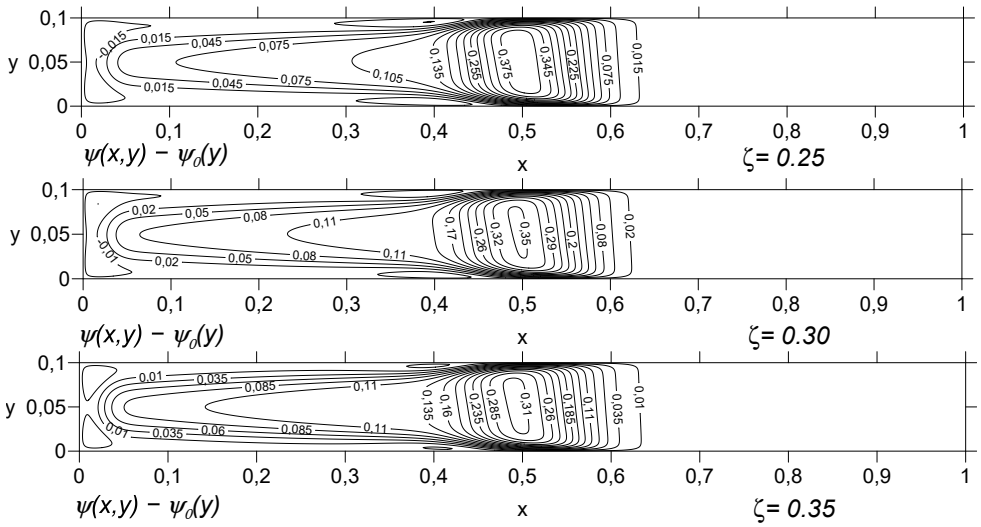

Figure 15: The fields of current function perturbation $(\psi - \psi_0)$, where $\psi_0 = \mathrm{Pe}\, y$. The calculation is performed for different values of clogging parameter (ζ), another parameter values are: $\mathrm{Pe} = 700$, $\mathrm{Rp} = 6000$, $a = 100$, $b = 1200$, $\phi_0 = 0.48$ at the dimensional time moment $t' = 480$ s.

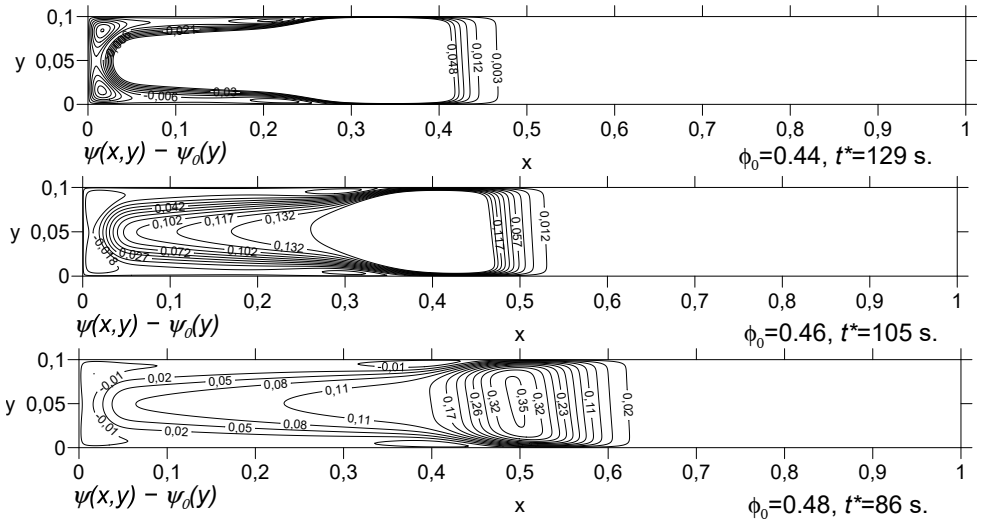

Figure 16: The fields of current function perturbation $(\psi - \psi_0)$, where $\psi_0 = \mathrm{Pe}\, y$. The calculation is performed for different values of clean media porosity (ϕ_0), another parameter values are: $\mathrm{Pe} = 700$, $\mathrm{Rp} = 6000$, $a = 100$, $b = 1200$, $\zeta = 0.3$ at the dimensional time moment $t' = 480$ s.

Appendix 1: The description of numerical method

The scheme is second-order accurate in space and first-order accurate in time. $c(x,y,t) = c^k_{i,j}$ $q(x,y,t) = q^k_{i,j}$, $\psi(x,y,t) = \psi^k_{i,j}$ where $t = k\tau$, $x = ih_x$, $y = jh_y$, $i = 0, ..., N-1$, $j = 0, ..., M-1$, $k = 0, ..., K$, $h_x = 1/(N-1)$, $h_y = 1/(M-1)$, $\tau = 1/K$. Let us write the systems of equations (12) in finite difference form. To calculate the mobile phase of the concentration is used ADI - alternate directions implicit method [22].

$$\frac{c_{i,j}^{k+1/2}-c_{i,j}^{k}}{\tau/2}+\frac{\zeta}{C_0}\frac{q_{i,j}^{k+1/2}-q_{i,j}^{k}}{\tau/2}=\frac{c_{i+1,j}^{k+1/2}-2c_{i,j}^{k+1/2}+c_{i-1,j}^{k+1/2}}{h_x^2}+\frac{c_{i,j+1}^{k}-2c_{i,j}^{k}+c_{i,j-1}^{k}}{h_y^2}$$
$$-\frac{\psi_{i,j+1}^{k}-\psi_{i,j-1}^{k}}{2h_y}\frac{c_{i+1,j}^{k+1/2}-c_{i-1,j}^{k+1/2}}{2h_x}+\frac{\psi_{i+1,j}^{k}-\psi_{i-1,j}^{k}}{2h_x}\frac{c_{i,j+1}^{k}-c_{i,j-1}^{k}}{2h_y},$$
$$\frac{c_{i,j}^{k+1}-c_{i,j}^{k+1/2}}{\tau/2}+\frac{\zeta}{C_0}\frac{q_{i,j}^{k+1}-q_{i,j}^{k+1/2}}{\tau/2}=\frac{c_{i+1,j}^{k+1/2}-2c_{i,j}^{k+1/2}+c_{i-1,j}^{k+1/2}}{h_x^2}+\frac{c_{i,j+1}^{k+1}-2c_{i,j}^{k+1}+c_{i,j-1}^{k+1}}{h_y^2} \tag{16}$$
$$-\frac{\psi_{i,j+1}^{k}-\psi_{i,j-1}^{k}}{2h_y}\frac{c_{i+1,j}^{k+1/2}-c_{i-1,j}^{k+1/2}}{2h_x}+\frac{\psi_{i+1,j}^{k}-\psi_{i-1,j}^{k}}{2h_x}\frac{c_{i,j+1}^{k+1}-c_{i,j-1}^{k+1}}{2h_y}.$$

Equation for the immobile component of concentration

$$\frac{q_{i,j}^{k+1}-q_{i,j}^{k}}{\tau}=a(c_{i,j}^{k+1}-q_{i,j}^{k+1}c_{i,j}^{k})-bq_{i,j}^{k+1}. \tag{17}$$

Equation for the current function

$$\frac{\psi_{i,j}^{n+1}-\psi_{i,j}^{n}}{\delta}=\frac{\psi_{i+1,j}^{n}-2\psi_{i,j}^{n}+\psi_{i-1,j}^{n}}{h_x^2}+\frac{\psi_{i,j+1}^{n}-2\psi_{i,j}^{n}+\psi_{i,j-1}^{n}}{h_y^2}-\kappa(q_{i,j}^{k})\mathrm{Rp}\frac{c_{i+1,j}^{k}-c_{i-1,j}^{k}}{2h_x}$$
$$+F(q_{i,j}^{k})\left(\frac{q_{i+1,j}^{k}-q_{i-1,j}^{k}}{2h_x}\frac{\psi_{i+1,j}^{n}-\psi_{i-1,j}^{n}}{2h_x}+\frac{q_{i,j+1}^{k}-q_{i,j-1}^{k}}{2h_y}\frac{\psi_{i,j+1}^{n}-\psi_{i,j-1}^{n}}{2h_y}\right), \tag{18}$$
$$\kappa(q_{i,j}^{k})=\frac{\phi_0^3(1-\zeta q_{i,j}^{k})^3}{(1-\phi_0(1-\zeta q_{i,j}^{k}))^2}\quad F(q_{i,j}^{k})=\frac{\zeta}{1-\zeta q_{i,j}^{k}}\left(\frac{3-\phi_0(1-\zeta q_{i,j}^{k})}{1-\phi_0(1-\zeta q_{i,j}^{k})}\right).$$

Systems of equations are reduced to a form convenient for solution. For the mobile component of concentration, the obtained equation is solved by the tridiagonal matrix algorithm [23]. For a half time step $k+1/2$ in the X-axis direction:

$$A_{i,j}c_{i-1,j}^{k+1/2}+B_{i,j}c_{i,j}^{k+1/2}+C_{i,j}c_{i+1,j}^{k+1/2}=F_{i,j}, \tag{19}$$

where

$$A_{i,j}=-\frac{\tau}{2h_x^2}-\frac{\tau}{4h_x}\frac{\psi_{i,j+1}^{k}-\psi_{i,j-1}^{k}}{2h_y},\quad B_{i,j}=1+\frac{\tau}{h_x^2}+\frac{\zeta}{C_0}\frac{a\tau/2}{1+\tau/2(ac_{i,j}^{k}+b)},$$
$$C_{i,j}=-\frac{\tau}{2h_x^2}+\frac{\tau}{4h_x}\frac{\psi_{i,j+1}^{k}-\psi_{i,j-1}^{k}}{2h_y},\quad F_{i,j}=\left(\frac{\tau}{2h_y^2}+\frac{\tau}{4h_y}\frac{\psi_{i+1,j}^{k}-\psi_{i-1,j}^{k}}{2h_x}\right)c_{i,j+1}^{k}$$
$$+\left(1-\frac{\tau}{h_y^2}\right)c_{i,j}^{k}+\left(\frac{\tau}{2h_y^2}-\frac{\tau}{4h_y}\frac{\psi_{i+1,j}^{k}-\psi_{i-1,j}^{k}}{2h_x}\right)c_{i,j-1}^{k}+\frac{\zeta}{C_0}\frac{\tau/2(ac_{i,j}^{k}+b)}{1+\tau/2(ac_{i,j}^{k}+b)},$$

and for a half time step $k+1$ in the Y-axis direction:

$$A_{i,j}c_{i-1,j}^{k+1}+B_{i,j}c_{i,j}^{k+1}+C_{i,j}c_{i+1,j}^{k+1}=F_{i,j}, \tag{20}$$

where

$$A_{i,j}=-\frac{\tau}{2h_y^2}+\frac{\tau}{4h_y}\frac{\psi_{i+1,j}^{k}-\psi_{i-1,j}^{k}}{2h_x},\quad B_{i,j}=1+\frac{\tau}{h_y^2}+\frac{\zeta}{C_0}\frac{a\tau}{1+\tau(ac_{i,j}^{k}+b)},$$
$$C_{i,j}=-\frac{\tau}{2h_y^2}-\frac{\tau}{4h_y}\frac{\psi_{i+1,j}^{k}-\psi_{i-1,j}^{k}}{2h_x},\quad F_{i,j}=\left(\frac{\tau}{2h_x^2}-\frac{\tau}{4h_x}\frac{\psi_{i,j+1}^{k}-\psi_{i,j-1}^{k}}{2h_y}\right)c_{i,j+1}^{k+1/2}$$
$$+\left(1-\frac{\tau}{h_x^2}+\frac{\zeta}{C_0}\frac{a\tau/2}{1+\tau/2(ac_{i,j}^{k}+b)}\right)c_{i,j}^{k+1/2}+\left(\frac{\tau}{2h_x^2}+\frac{\tau}{4h_x}\frac{\psi_{i,j+1}^{k}-\psi_{i,j-1}^{k}}{2h_y}\right)c_{i,j-1}^{k+1/2}$$
$$+\frac{\zeta}{C_0}\frac{\tau/2(ac_{i,j}^{k}+b)}{(1+\tau(ac_{i,j}^{k}+b))(1+\tau/2(ac_{i,j}^{k}+b))},$$

and equation (17) will be of the form

$$q_{i,j}^{k+1} = \frac{a\tau c_{i,j}^{k+1} + q_{i,j}^{k}}{1 + \tau(ac_{i,j}^{k} + b)}. \tag{21}$$

Richardson's scheme [24] is used to solve the equation for the current function. The original elliptic equation is treated as a parabolic equation. The parabolic equation is solved by an explicit scheme using fictitious time. The calculation is carried out to a given accuracy.

$$\begin{aligned}\psi_{i,j}^{n+1} &= \delta\left[\left(\frac{1}{h_x^2} + F(q_{i,j}^{k})\frac{q_{i+1,j}^{k} - q_{i-1,j}^{k}}{4h_x^2}\right)\psi_{i+1,j}^{n} + \left(\frac{1}{h_x^2} - F(q_{i,j}^{k})\frac{q_{i+1,j}^{k} - q_{i-1,j}^{k}}{4h_x^2}\right)\psi_{i-1,j}^{n}\right] \\ &+ \delta\left[\left(\frac{1}{h_y^2} + F(q_{i,j}^{k})\frac{q_{i,j+1}^{k} - q_{i,j-1}^{k}}{4h_y^2}\right)\psi_{i,j+1}^{n} + \left(\frac{1}{h_y^2} - F(q_{i,j}^{k})\frac{q_{i,j+1}^{k} - q_{i,j-1}^{k}}{4h_y^2}\right)\psi_{i,j-1}^{n}\right] \\ &+ \left[1 - \delta\left(\frac{2}{h_x^2} + \frac{2}{h_y^2}\right)\right]\psi_{i,j}^{n} - \delta\kappa(q_{i,j}^{k})\mathrm{Rp}\frac{c_{i+1,j}^{k} - c_{i-1,j}^{k}}{2h_x},\end{aligned} \tag{22}$$

here δ is fictitious time step.

$$\left|\frac{\psi_{i,j}^{n+1} - \psi_{i,j}^{n}}{\psi_{i,j}^{n+1}}\right| < \epsilon, \tag{23}$$

here ϵ is a target accuracy.

The boundary conditions (13) in finite-difference form are

$$\begin{aligned}&c_{0,j}^{k} = \frac{(\psi_{0,j+1}^{k} - \psi_{0,j}^{k})h_x/h_y\, f(k) + c_{0,j}^{k}}{(\psi_{0,j+1}^{k} - \psi_{0,j}^{k})\, h_x/h_y + 1}, \quad f(k) = \begin{cases}1 & \text{if } k \le k_c \\ 0 & \text{if } k > k_c\end{cases} \\ &c_{N-1,j}^{k} = c_{N-2,j}^{k}, \quad c_{i,0}^{k} = c_{i,1}^{k}, \quad c_{i,M-1}^{k} = c_{i,M-2}^{k}, \\ &\psi_{0,j}^{k} = \mathrm{Pe}\, h_y j, \quad \psi_{N-1,j}^{k} = \mathrm{Pe}\, h_y j, \quad \psi_{i,M-1}^{k} = \mathrm{Pe}\, h_y (M-1), \quad \psi_{i,0}^{k} = 0.\end{aligned}$$

Initial conditions (14) are set by absence of impurity inside the region and constant filtration rate in form of

$$c_{i,j}^{0} = 0, \quad q_{i,j}^{0} = 0, \quad \psi_{i,j}^{0} = \mathrm{Pe}\, h_y j, \quad i = 0, ..., N-1, \quad j = 0, ..., M-1.$$

References

[1] Agbangla, G.C., Climent, E., Bacchin, P., *Experimental Investigation of Pore Clogging by Microparticles: Evidence for a Critical Flux Density of Particle Yielding Arches and Deposits*, Sep. Purif. Technol., 101 (2012), 42-48.

[2] Zagoruiko A., Mikenin P., *Decomposition of hydrogen sulfide into elements in the cyclic chemisorption-catalytic regime*, Catalysis Today, 378 (2021), 176-188.

[3] Zheng, X.L., Shan, B.B., Chen, L., Sun, Y.W., Zhang, S.H., *Attachment-detachment dynamics of suspended particle in porous media: experiment and modeling*, J. Hydrol., 511 (2014), 199-204.

[4] Klimenko L.S., Maryshev B.S., *Numerical Simulation of Microchannel Blockage by the Random Walk Method*, Chem. Eng. J., 381 (2020), 122644.

[5] Deans H. A. , *A mathematical model for dispersion in the direction of flow in porous media*, Society of Petroleum Engineers Journal, 3.1 (1963), 49-52.

[6] Einstein A., *Zur theorie der brownschen bewegung*, Ann. Phys., Vol.324 Issue 2 (1906), p.371-381.

[7] Van Genuchten, MTh., Wierenga P.J., *Mass transfer studies in sorbing porous media I. Analytical solutions*, Soil Sci. Soc. Am. J., 40.4 (1976), 473-480.

[8] Bromly M., Hinz C., *Non-Fickian transport in homogeneous unsaturated repacked sand*, Water Resour. Res., 40 (2004), W07402.

[9] Gouze P., Le Borgne T., Leprovost R., Lods G., Poidras T., Pezard P., *Non-Fickian dispersion in porous media: 1. Multiscale measurements using single-well injection withdrawal tracer tests*, Water Resour. Res., 44.6 (2008), W06426.

[10] Selim H., *Prediction of contaminant retention and transport in soils using kinetic multireaction models*, Environ. Health Perspect., 83 (1989), 69-75.

[11] Maryshev B. S., Khabin M. R., Evgrafova A. V., *Identification of transport parameters for the solute filtration through porous media with clogging*, Journal of Porous Media, 26.6 (2023), 31-53.

[12] Zaheer M., Wen Z., Zhan H., Chen X., Jin M. , *An experimental study on solute transport in one‐Ђђdimensional clay soil columns*, Geofluids, 2017.1 (2017), 6390607.

[13] Lu B., Zhang Y., Zheng C., Green C. T., O'Neill C., Sun H. G., Qian J., *Comparison of time nonlocal transport models for characterizing non-Fickian transport: From mathematical interpretation to laboratory application*, Water., 10.6 (2018), 778.

[14] Younes A., Zaouali J., Kanzari S., Lehmann F., Fahs M., *Bayesian simultaneous estimation of unsaturated flow and solute transport parameters from a laboratory infiltration experiment*, Water., 11.8 (2019), 1660.

[15] Schincariol R. A., Schwartz F. W., *An experimental investigation of variable density flow and mixing in homogeneous and heterogeneous media*, Water Resources Research, 26.10 (1990), 2317-2329.

[16] Burns P. J., Chow L. C., Tien C. L., *Convection in a vertical slot filled with porous insulation*, International Journal of Heat and Mass Transfer, 20.9 (1977), 919-926.

[17] Maryshev B. S., Klimenko L. S., *Cleaning porous media by an external vertical flow*, Acta Mechanica., 234.8 (2023), 3305-3320.

[18] Nield Donald A., Adrian Bejan, *Convection in porous media*, New York: springer, 2017.

[19] Carman, P.C., *Fluid flow through a granular bed*, Trans. Inst. Chem.Eng. London, 15 (1937), 150-156.

[20] Guo W., Langevin C.D., *User's guide to SEAWAT: a computer program for simulation of three-dimensional variable-density ground-water flow*, US Geological Survey, 2002.

[21] Maryshev B.S., *The linear stability of vertical mixture seepage into the close porous filter with clogging*, Fluid Dyn. Res., 49.1 (2016), 015501.

[22] Simoncini V., *Computational Methods for Linear Matrix Equations*, siam REVIEW, 58.3 (2016), 377-441.

[23] Thomas L.H. , *Elliptic problems in linear difference equations over a network*, Watson Sci. Comput. Lab. Rept., Columbia University, New York, 1949.

[24] Roache P. J. , *Computational fluid dynamics*, Albuquerque, NM: Hermosa Publishers, 1972.

Mikhail R. Khabin,
Institute of Continuous Media Mechanics (ICMM UB RAS),
Academika Korolev st. 1, 614013 Perm, Russia
Email: mikhail.khabin@mail.ru

Anna V. Belyaeva,
Institute of Continuous Media Mechanics (ICMM UB RAS),
Academika Korolev st. 1, 614013 Perm, Russia
Email: eav@icmm.ru

Boris S. Maryshev,
Institute of Continuous Media Mechanics (ICMM UB RAS),
Academika Korolev st. 1, 614013 Perm, Russia
Email: bmaryshev@icmm.ru

Received 30.10.2024 , Accepted 25.05.2025, Available online 31.12.2025